Supporting Information

Passon et al. 10.1073/pnas.1120792109

SI Methods

Expression, Purification, and Crystallization of PSPC1/NONO Heterodimer. Briefly, truncated constructs of PSPC1 (residues 61–320 relative to UniProt entry PSPC1_HUMAN) and NONO (53-312 of NONO_HUMAN) were ligated into the pET-Duet1 vector (Novagen). Coexpression in Rosetta2 (DE3) *Escherichia coli* cells (Novagen) results in 10-mg/L yields of heterodimer that can be purified by nickel-affinity chromatography using a tobacco etch virus protease-cleavable hexahistidine tag fused to PSPC1. Subsequent gel filtration and centrifugal concentration yields protein samples suitable for crystallization and biophysical study. Crystals are obtained from hanging-drop vapor diffusion experiments using a reservoir solution of 0.5 M NaCl, 0.1 M Bis-Tris (pH 5.5), 28% (wt/vol) PEG 3350 (native), or 0.5 M NaCl, 0.1 M Bis-Tris (pH 5.5), and 18% (wt/vol) PEG 3350 (SeMet), and typically diffract to >2.0 Å resolution in space group *C2* (a = 90.90, b = 67.18, c = 94.08 Å, β = 99.96°), on beamline MX2 of the Australian Synchrotron.

Small-Angle X-Ray Scattering. Small-angle X-ray scattering (SAXS) experiments were carried out at the SAXSWAXS beamline of the Australian Synchrotron. Scattering from a dilution series [12, 6, 3, 1.5, 0.75, 0.375 mg/mL of protein in 50 mM Tris·HCl (pH 7.5) and 150 mM NaCl] was carried out using ten 2-s exposures of solution flowing through a 1.5-mm quartz capillary. Data were collected on a Pilatus 6M detector and processed using SAXS15ID. Blank-subtracted and averaged data were exported for analysis with the ATSAS suite (1). A radius of gyration was determined to be 29.34 ± 0.057 Å and Dmax to be 85.5 Å (Fig. S2). Despite evidence of a minor component of aggregated protein in the sample, CRYSOL was used to compare favorably the observed scattering with that calculated from the crystallographic model.

Plasmids for Fluorescent Protein Fusions. pEYFP_NLS-PSPC1 61–312, 320, 325, 330, 335, 340, 345, 350, and 355 plasmids were all made by ligating inserts generated by PCR using pEYFP-C1-PSPC1 (human) as a template, and the appropriate primers with engineered EcoRI (5′) and BamHI (3′) sites for cloning, into pEYFP_NLS plasmid backbone using the same sites. pEYFP_NLS plasmid was generated by ligation of an engineered annealed DNA oligo containing the SV40 large T-antigen nuclear localization signal into the BglII restriction enzyme site within the multicloning site of the pEYFP-C1 plasmid (Clontech), maintaining both the ORF as well as BglII sites at either end of the insert. pEYFP_NONO Y267A/W271A was made by QuikChange site-directed mutagenesis (Stratagene) using complementary oligonucleotides containing the base-pair substitutions and the template plasmid pEYFP-C1-NONO (human). pmCherry-PSPC1-Y275A/W279A was made by QuikChange site-directed mutagenesis using complementary oligonucleotides containing the base-pair substitutions and the template plasmid pmCherry-PSPC1. For yeast two-hybrid analyses, wild-type and mutant PSPC1 and NONO were amplified from the plasmids generated above and cloned into the AscI and NotI sites of pGBK-RC and pGAD-RC.

Localization Assays and Immunoprecipitation. HeLa cells were grown in DMEM supplemented with 10% (vol/vol) FCS and 1% penicillin streptomycin (Invitrogen). Transfections were performed using Lipofectamine 2000 according to the manufacturer's instructions (Invitrogen). Typically, cells were analyzed 16–18 h posttransfection; however, only cells with low levels of expression were imaged, because overexpression of PSPC1 and its derivatives causes mislocalization of the protein to unspecific nuclear aggregates. For microscopy assays, cells were grown on glass coverslips and fixed in 4% (wt/vol) paraformaldehyde in PBS for 5 min on ice. Selected coverslips were incubated on ice in 0.1% Triton X-100 (in PBS) for 5 min before fixation, to remove soluble fluorescent protein. Where endogenous paraspeckles needed to be visualized, immunostaining was carried out as described (2) with anti-NONO monoclonal antibody (3) and anti-mouse TRITC secondary antibody (Jackson). Before mounting, cells were stained with DAPI (0.3 μg/mL; Sigma) for 1 min and then mounted using Vectashield (Vector Laboratories). Z-stacks of cells were obtained using a Nikon Ti-E inverted wide-field fluorescence microscope, followed by deconvolution (Autoquant). Images are individual slices through a cell unless stated otherwise.

Cell lysates were prepared from transfected HeLa cells using RIPA buffer [50 mM Tris (pH 7.5), 0.5 M NaCl, 1% Nonidet P-40, 1% DOC, 0.1% SDS, and 2 mM EDTA with complete protease inhibitors] followed by shearing of the DNA in a QIAshredder (Qiagen). Immunoprecipitation was carried out with GFP-TRAP magnetic beads (ChromoTek). Briefly, lysates were precleared with protein G Dynabeads, and GFP-TRAP beads were added. The beads were rotated at 4 °C overnight in lysate followed by two RIPA buffer washes and two washes in 50 mM Tris (pH 7.5), 150 mM NaCl, and 0.05% Igepal. Beads were then heated in LDS loading dye, and resulting protein samples subject to electrophoresis and Western blotting with anti-GFP (Roche) and anti-NONO followed by anti-mouse peroxidase (GE Healthcare) and detection with Luminata Forte chemiluminescence reagent (Millipore).

Yeast Two-Hybrid Analyses. Yeast strains PJ69–2A (*MAT*a, *trp1–901*, *leu2–3, 112, ura3–52*, *his3Δ200*, *gal4Δ*, *gal80Δ*, *GAL2*::*ADE2*, *GAL1*::*HIS3*) and MaV204K (*MAT*α, *trp1–901, leu2–3, 112, his3Δ200*, *ade2–101Δ*::*kanMX*, *gal4Δ*, *gal80Δ*, *SPAL10*::*URA3*, *UASGAL1*::*HIS3*, *GAL1*::*lacZ*) were transformed with the GAL4 DNA-binding domain fusions in pGBK-RC and GAL4 activation domain fusions in pGAD-RC, respectively, using the LiAc method according to Gietz and Woods (4). Yeast expressing DNA-binding domain fusions were mated with yeast expressing GAL4 activation domain fusions by mixing equal amounts of cells and incubating them overnight on YPAD agar. Diploid cells were selected on synthetic complete (SC) agar lacking leucine and tryptophan and dotted onto SC media lacking adenine, histidine, leucine, tryptophan, and uracil, supplemented with 50 mM 3-aminotriazole, to test for protein: protein interactions.

1. Svergun DI (1992) Determination of the regularization parameter in indirect-transform methods using perceptual criteria. *J Appl Cryst* 25:495–503.
2. Fox AH, et al. (2002) Paraspeckles: A novel nuclear domain. *Curr Biol* 12:13–25.
3. Souquere S, Beauclair G, Harper F, Fox A, Pierron G (2010) Highly ordered spatial organization of the structural long noncoding NEAT1 RNAs within paraspeckle nuclear bodies. *Mol Biol Cell* 21:4020–4027.
4. Gietz RD, Woods RA (2006) Yeast transformation by the LiAc/SS Carrier DNA/PEG method. *Methods Mol Biol* 313:107–120.

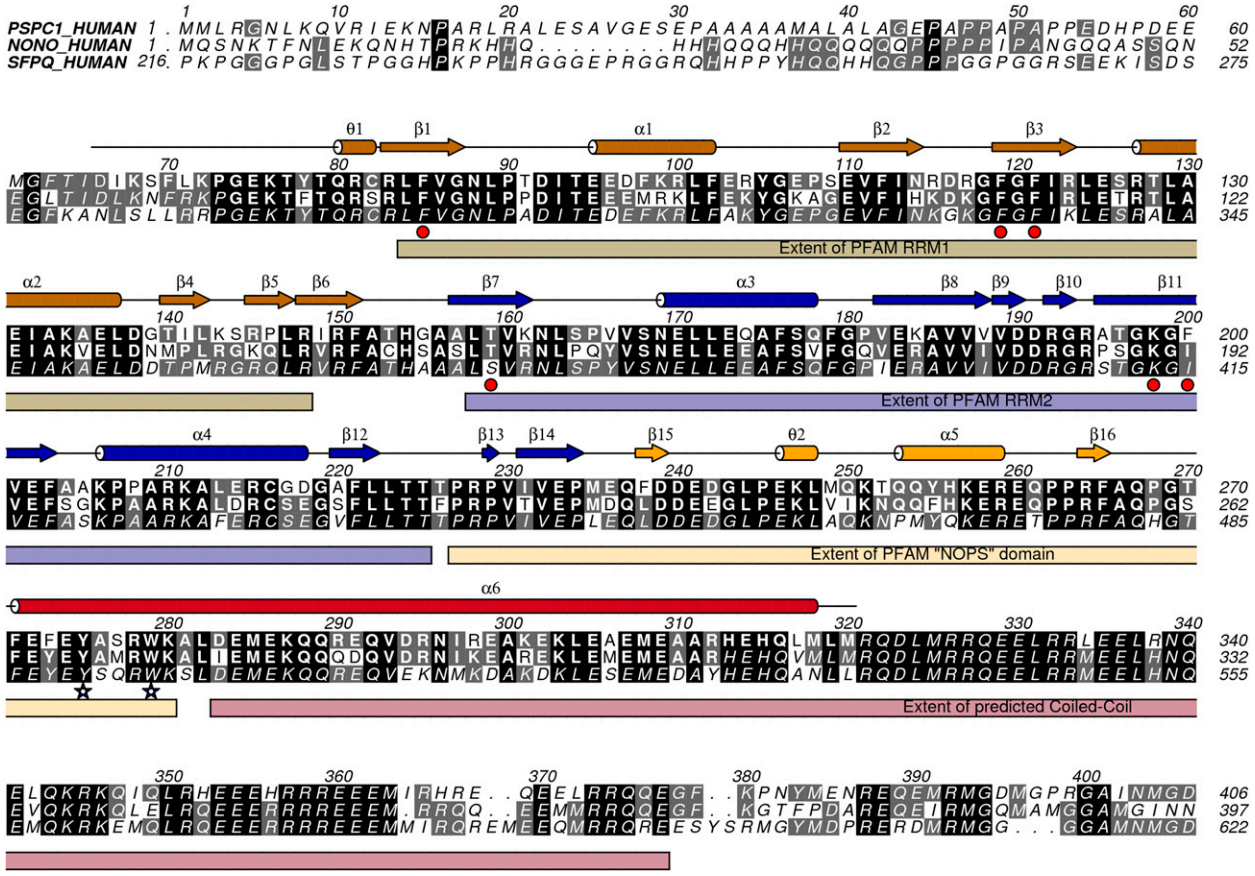

Fig. S1. Sequence alignment encompassing the conserved region of human *Drosophila* behavior/human splicing proteins (DBHS; labeled by UniProt ID) shaded according to sequence similarity. Amino acids in italics were not observed in the crystal structure. A consensus secondary structure scheme is marked based on the structure described herein, and colored by domain. Domain definitions are provided on a separate line. Red circles indicate canonical RNA-binding residues. Stars indicate the position of residues mutated in double mutants. Produced with ALINE (1).

1. Bond CS, Schüttelkopf AW (2009) ALINE: A WYSIWYG protein-sequence alignment editor for publication-quality alignments. *Acta Crystallogr D Biol Crystallogr* 65:510–512.

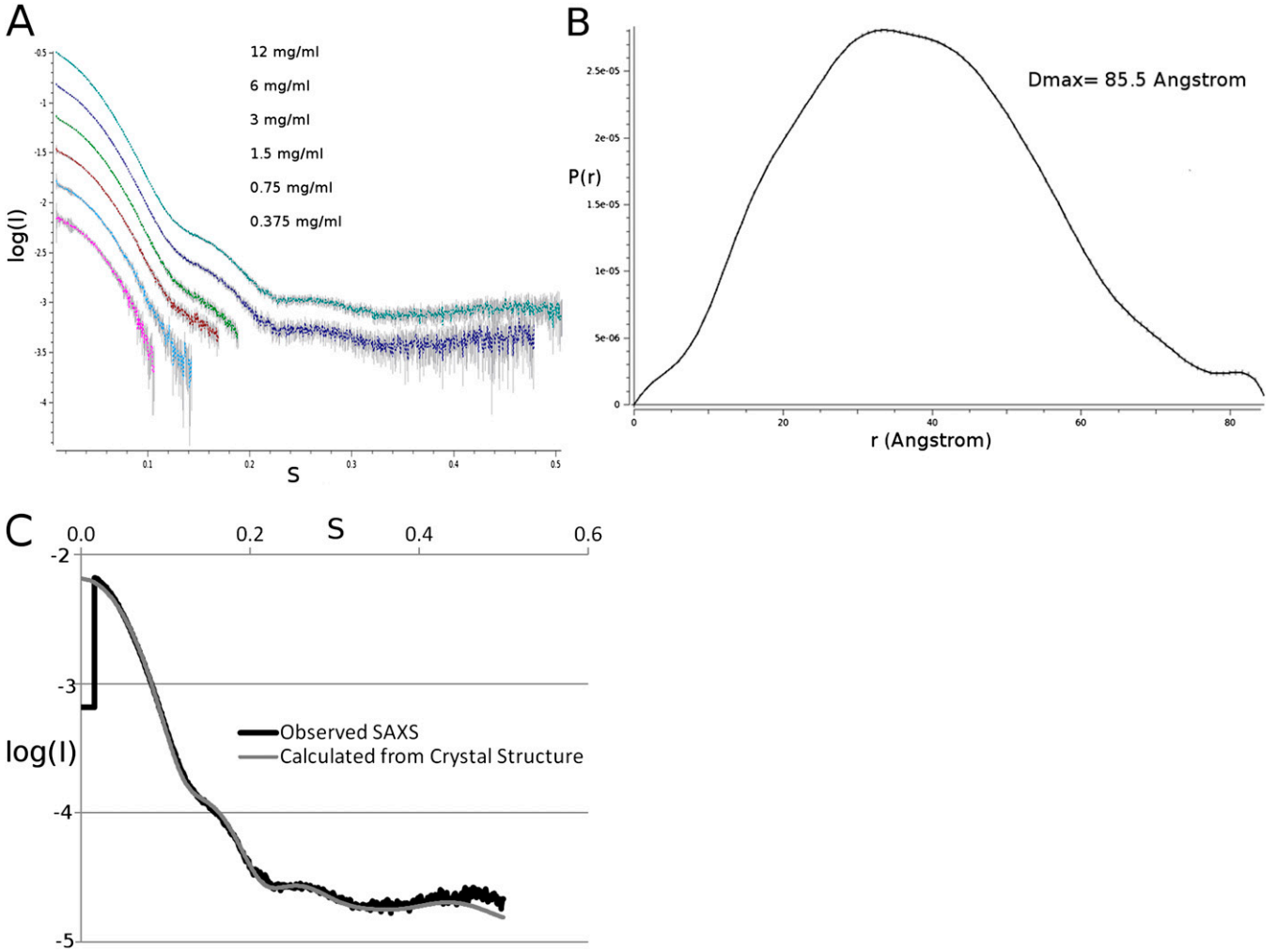

Fig. S2. SAXS analysis of the PSPC1/NONO heterodimer. (*A*) Background-subtracted SAXS for a concentration series. (*B*) Distance distribution of data merged from *A* leads to estimation of maximum dimension of 85.5 Å, which corresponds well to the crystal structure. (*C*) Comparison of observed X-ray scattering with that calculated from the crystal structure with CRYSOL, indicating a close match between observed solution scattering and scattering obtained from our model.

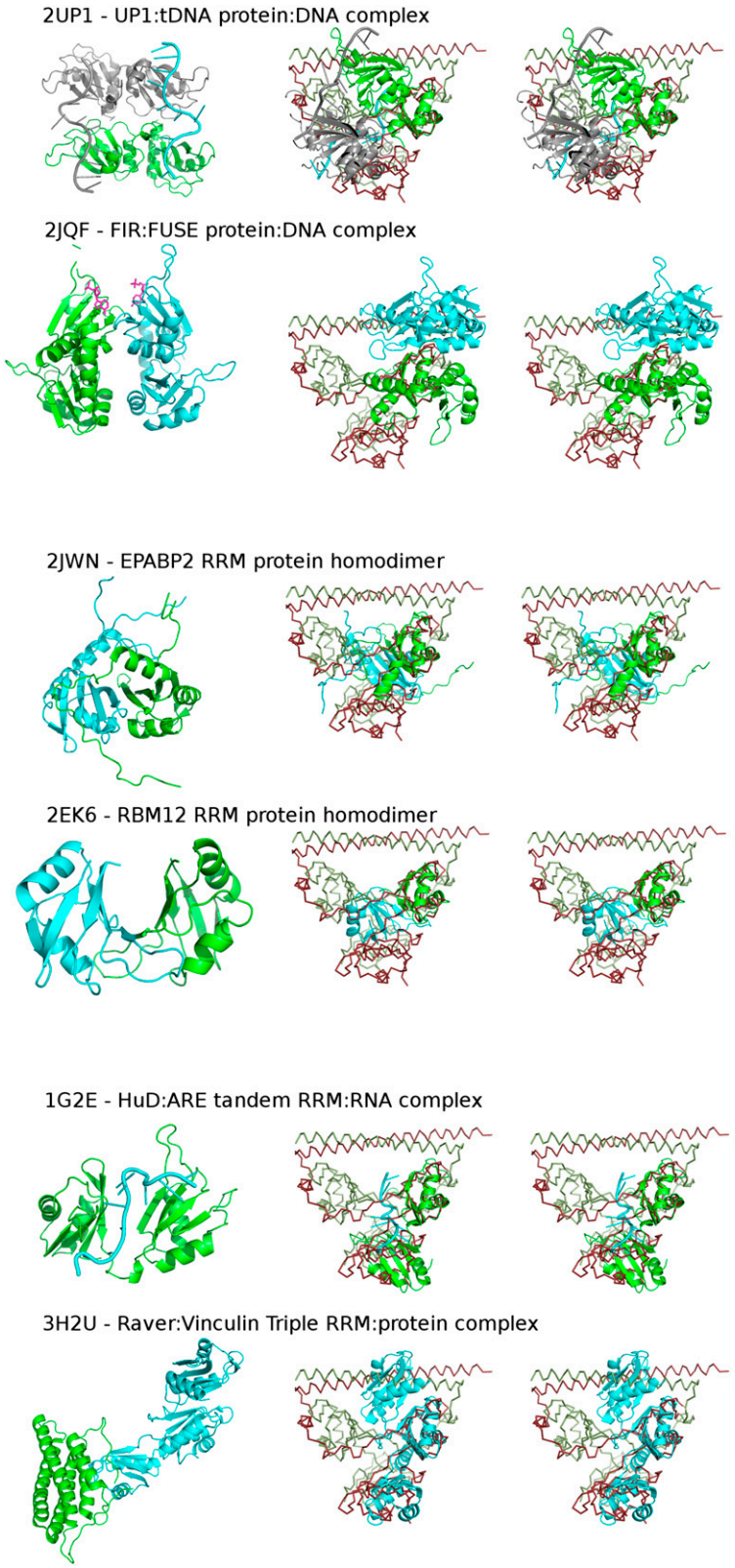

Fig. S3. Structural comparison of the PSPC1/NONO heterodimer with other oligomeric or tandem RNA recognition motif (RRM) structures. (*Left*) Structure in question in cartoon mode. (*Right*) Stereoscopic view of the optimal superposition of the structure (cartoon) on the PSPC1/NONO heterodimer (red and green Cα trace). UP1:tDNA (1) and FUSE:FIR (2) are examples of homodimers of tandem RRM proteins. EPABP2 (3) and RBM12 (PDB ID code 2EK6) are examples of homodimers of RRM domains. HuD:ARE (4) and Raver (5) are examples of monomeric tandem RRM domains.

1. Ding J, et al. (1999) Crystal structure of the two-RRM domain of hnRNP A1 (UP1) complexed with single-stranded telomeric DNA. *Genes Dev* 13:1102–1115.
2. Crichlow GV, et al. (2008) Dimerization of FIR upon FUSE DNA binding suggests a mechanism of c-myc inhibition. *EMBO J* 27:277–289.
3. Song J, McGivern JV, Nichols KW, Markley JL, Sheets MD (2008) Structural basis for RNA recognition by a type II poly(A)-binding protein. *Proc Natl Acad Sci USA* 105:15317–15322.
4. Wang X, Tanaka Hall TM (2001) Structural basis for recognition of AU-rich element RNA by the HuD protein. *Nat Struct Biol* 8:141–145.
5. Lee JH, Rangarajan ES, Yogesha SD, Izard T (2009) Raver1 interactions with vinculin and RNA suggest a feed-forward pathway in directing mRNA to focal adhesions. *Structure* 17: 833–842.

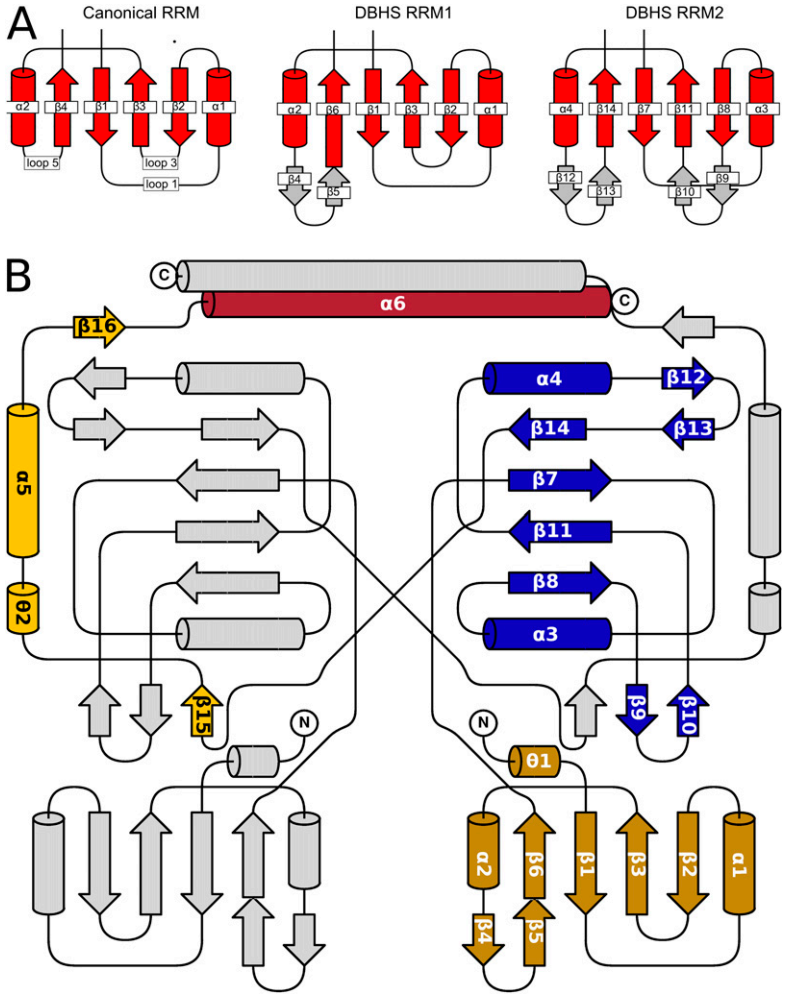

Fig. S4. (*A*) Correspondence of canonical RRM secondary structure nomenclature and topology with the DBHS RRM domains. (*B*) Complete topology of the PSPC1/NONO heterodimer. Colors correspond to Fig. 1. Prepared with TOPDRAW (1).

1. Bond CS (2003) TopDraw: A sketchpad for protein structure topology cartoons. *Bioinformatics* 19:311–312.

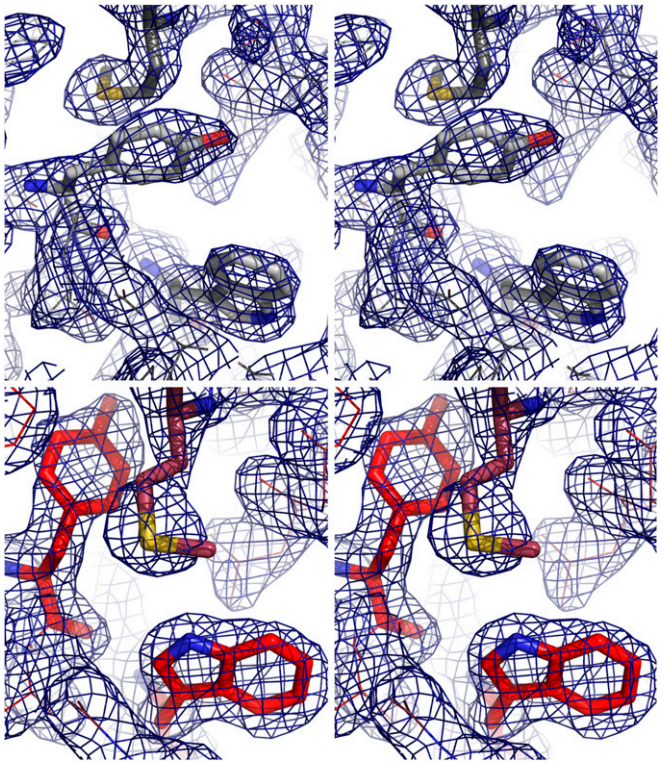

Fig. S5. Electron density provides evidence for the different structures of conserved Met, Tyr, and Trp residues described in Fig. 2. Stereoscopic representation of σ-weighted 2mFo-DFc electron density at 1 SD (blue mesh) superimposed onto the two relevant regions of the structure.

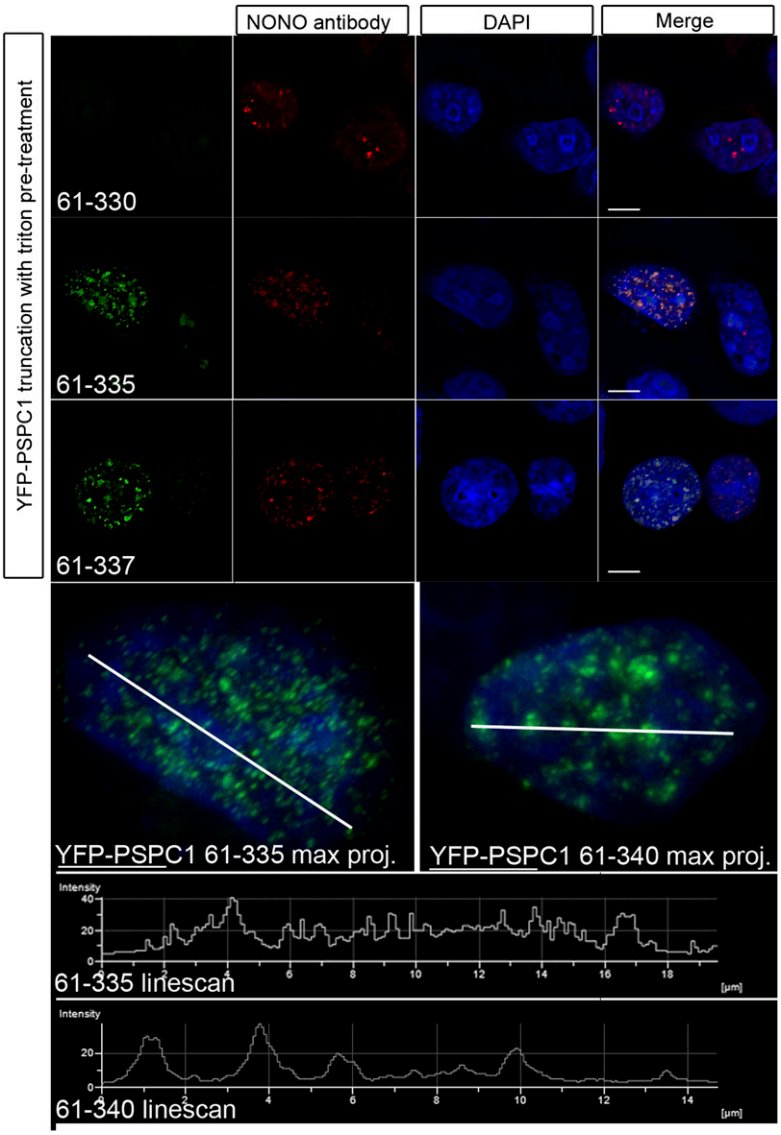

Fig. S6. The extended coiled-coil region of PSPC1 is required for paraspeckle formation. Fluorescent micrographs of HeLa cells, extracted with detergent before fixation to reveal any underlying sub-structures, transfected with plasmids encoding YFP-PSPC1 truncation proteins (green) residues 61–330, 61–335, and 61–337 (*Top* three rows), costained with anti-NONO (red), and stained with DAPI (blue). Line scans (*Bottom* three rows) show the difference between the microspeckles seen with protein terminating at 335, and the large paraspeckles seen in the protein terminating at residue 340. Microspeckles are only apparent for proteins ending at 335 or 336, indicating a small gradient of transitional localization from diffuse (e.g., protein ending at 330) to paraspeckles (protein ending at 337). (Scale bars: 5 µm.)

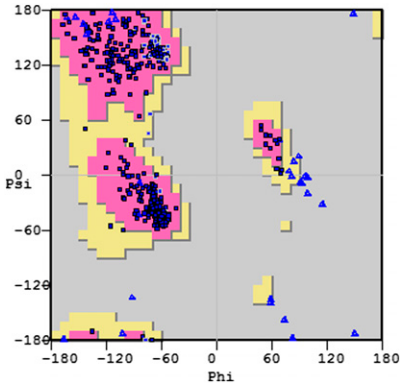

Fig. S7. Ramachandran analysis of the PSPC1/NONO dimer.

Table S1. Crystallographic, refinement, and model statistics

Space group	*C 1 2 1*
Cell dimensions, Å, °	a = 90.90, b = 67.18, c = 94.08, β = 99.96
Solvent content, %	47
Resolution range, Å	19.4–1.9
Unique reflections (R_{free} set)	43,468 (2,206)
Final R factor (R_{free})	0.183 (0.228)
No. of protein, ligand, water atoms	4,020, 11, 437
B value, protein, ligand, water, Å^2	41.6, 61.0, 49.0
Rmsd bond lengths, angles, Å,°	0.01, 1.05
MolProbity score	1.16 (100% centile)

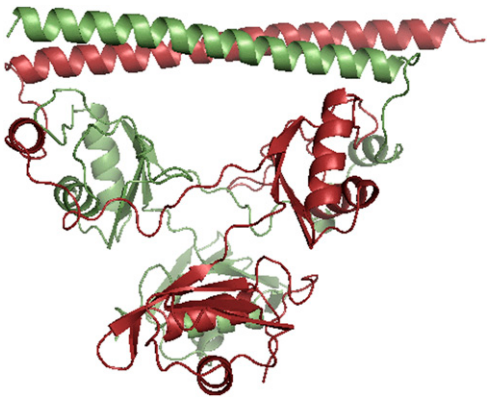

Movie S1. A ribbon representation of the PSPC1 (red)/NONO (green) heterodimer rotating around the *y* axis and then the *x* axis.

Movie S1